Geoscience Frontiers 8 (2017) 1025–1037

HOSTED BY

Contents lists available at ScienceDirect

China University of Geosciences (Beijing)

Geoscience Frontiers

journal homepage: www.elsevier.com/locate/gsf

Research paper

Geochemistry and Sm-Nd systematics of the 1.67 Ga Buanji Group of southwestern Tanzania: Paleo-weathering, provenance and paleo-tectonic setting implications

Charles H. Kasanzu*, Makenya A.H. Maboko, Shukrani Manya

Department of Geology, University of Dar es Salaam, P.O. Box 35052, Dar es Salaam, Tanzania

ARTICLE INFO

Article history:
Received 30 May 2016
Received in revised form
21 August 2016
Accepted 7 September 2016
Available online 2 November 2016

Keywords:
Buanji Group
Shales
Source weathering conditions
Provenance

ABSTRACT

We present major and trace and Nd-isotopic data of the ~1.67 Ga Buanji Group of southwestern Tanzania in order to constrain the nature of their protolith and the intensity of chemical weathering in the source terranes and make inferences on the nature of climatic conditions during the late Paleoproterozoic in the region. Major and trace element contents of the shales from three stratigraphic formations are comparable to those of the post-Archaean Australian Shale (PAAS) and the average Proterozoic Shale (PS). They are characterized by enrichments in LREE relative to HREE ($(La/Yb)_{CN} = 9.07-13.2$; $(Gd/Yb)_{CN} = 1.51-1.85$) and negative Eu anomalies ($Eu/Eu^* = 0.61-0.81$); features which are comparable to those of PAAS and PS, indicating upper continental sources. Provenance proxy ratios, together with abundances of Cr, Ni, Co and V that increase up-stratigraphy suggest a decreasing input of felsic detritus up-stratigraphy. Chemical Indices of Alteration (CIA) for the lower, middle and upper Buanji formations are 81, 76 and 79, respectively. These indices largely indicate intermediate (ca. 60–80) to extreme (>80) weathering intensities of the precursor rocks. These observations may suggest the prevalence of warm, humid climates during the late Paleoproterozoic in the region.

The lower Buanji Formation yielded a depleted mantle Nd model age (T_{DM}) of ~2100 Ma which indicates an Eburnean parentage. T_{DM} ages of 2486–2155 Ma and 2535–2379 Ma obtained from middle and upper Buanji formations, respectively, suggest a progressive increase of sedimentary input from the Tanzania Craton up-stratigraphy. The Eburnean T_{DM} ages of the lower Buanji rocks are attributed to their derivation through denudation of a decaying topographic high composed predominantly of rocks that were generated during the Palaeoproterozoic Ubendian orogenesis, possibly in the realm of Columbian Supercontinent assembly. Overlapping T_{DM} ages between the middle and upper Buanji formations suggest multiple sources involving mixing of detritus from Archaean cratonic rocks and the Palaeoproterozoic Ubendian belt. However, the Archaean signal is relatively more pronounced in the upper Buanji Formation, suggesting sediments derivation from the craton, to the north of the basin. The middle Buanji Formation suggests more diverse protolith, given the relatively larger spread in the T_{DM} ages. The Nb/Ta, Zr/Sm and Ce/Pb ratios coupled with the negative Nb and Ta anomalies, relative to primitive mantle, suggest that the tectonic setting of the source rocks for the Buanji sediments was a subduction zone akin to that generating modern Island Arc Basalts. Thus, we suggest that the Buanji's palaeogeography is consistent with an extensional continental backarc basin during the late Paleoproterozoic.

© 2016, China University of Geosciences (Beijing) and Peking University. Production and hosting by Elsevier B.V. This is an open access article under the CC BY-NC-ND license (http://creativecommons.org/licenses/by-nc-nd/4.0/).

1. Introduction

Geochemical studies of clastic sedimentary rocks in ancient basins can be used to reconstruct sediment sources, tectonism and the physico-chemical conditions that prevailed during deposition and make inferences on past climates (Nesbitt and Young, 1982; Taylor and McLennan, 1985; Nagarajan et al., 2007; Shao et al.,

* Corresponding author. Fax: +255 22 2410481.
E-mail address: kcharls16@yahoo.com (C.H. Kasanzu).
Peer-review under responsibility of China University of Geosciences (Beijing).

http://dx.doi.org/10.1016/j.gsf.2016.09.004
1674-9871/© 2016, China University of Geosciences (Beijing) and Peking University. Production and hosting by Elsevier B.V. This is an open access article under the CC BY-NC-ND license (http://creativecommons.org/licenses/by-nc-nd/4.0/).

2012). This is made possible by the fact that these rocks furnish information on the chemistry of hinterlands even when the protolith rocks themselves may have been completely eroded (Taylor and McLennan, 1985; Roddaz et al., 2006; Servaraj and Arthur, 2006; Kasanzu et al., 2008; Ali et al., 2014). This approach has been applied to various clastic sedimentary basins ranging in age from the Archaean (e.g., Abitibi greenstone belt, Canada; Feng and Kerrich, 1990), Proterozoic (e.g., Ikorongo Group, Tanzania; Kasanzu et al., 2008), Cambrian–Ordovician (e.g., Central Asian Orogenic Belt, Mongolia; Chen et al., 2014), Palaeozoic (e.g., Xing-Meng Orogenic Belt, Mongolia; DaPeng et al., 2011) and Mesozoic (e.g., Olduvai and Laetoli, Tanzania; Kasanzu et al., 2016a). The use of clastic sedimentary rocks geochemistry in this context is based on the chemical behaviour of the rare earth, trace and some major elements whose abundances are not affected for most fine-grained sedimentary rocks during weathering, erosion and transportation (Taylor and McLennan, 1985; Kasanzu et al., 2008). Additionally, the effect of density and/or grain size induced by sedimentary sorting is trivial for ratios of immobile trace elements in shales, mudstones and siltstones (e.g., McLennan, 1989).

The Buanji Group of southwestern Tanzania (Figs. 1 and 2) represents clastic sedimentary deposits that date back to the late Paleoproterozoic (Manya, 2013). These strata are cross-cut by effusive volcanism represented by amygdaloidal lavas at the summit of the stratigraphic section (Figs. 2 and 3). The sedimentary rocks associated with the lavas are conglomerates, quartzites, brown and green shales, dolomites, micaceous siltstones and sandstones. These rocks unconformably overlie a basement composed of the ~1.8–2.0 Ga Ubendian high grade metamorphic rocks, anorthosites, gabbros and granitic intrusives (Lenoir et al., 1994). The green shales of the Buanji Group host Cu mineralization which has attracted the attention of artisanal miners. Despite its economic potential, modern geochemical work is limited to the work of (2013) who reported a zircon U-Pb age of 1674 ± 15 Ma for the andesitic lavas; the age which is interpreted to represent the minimum age of deposition for the underlying sedimentary rocks. In this paper, we report major, trace elements and Sm-Nd data to the sedimentary rocks of the Buanji Group with a view to constraining the nature of the protolith, the intensity of chemical weathering in the source terranes and make inferences on climatic conditions that prevailed in the region during deposition.

2. Geological setting

The Precambrian geology of southwestern Tanzania is dominated by high grade metamorphic rocks of the Eburnean Ubendian orogen which include micaceous schists, gneisses and migmatites, garnetiferous quartzites, eclogites and marbles (Boniface et al., 2012; Kazimoto et al., 2015). These rocks are considered to be of sedimentary origin that underwent profound regional metamorphism and migmatization in the realm of Columbia supercontinent assembly (Lenoir et al., 1994; Boven et al., 1999; Zhao et al., 2004). The high-grade rocks have been intruded by widespread granitoids including granodiorites and K-rich granites that are dated between ca. 1.96 and 1.85 Ga (Manya, 2011, 2012, 2014; Lawley et al., 2013; Kazimoto et al., 2015; Tulibonywa et al., 2015; Bahame et al., 2016).

Lying unconformably on the Ubendian rocks are low grade metasedimentary rocks of the Ukingan Supergroup and the sedimentary deposits of the Buanji Group (Fig. 2). The largely sedimentary rocks of the Buanji Group are divided into lower, middle and upper formations with a maximum thickness of approximately 245 m, 366 m and 457 m, respectively (Harpum and Brown, 1958; Manya, 2013). The lower Formation is comprised of ripple-marked

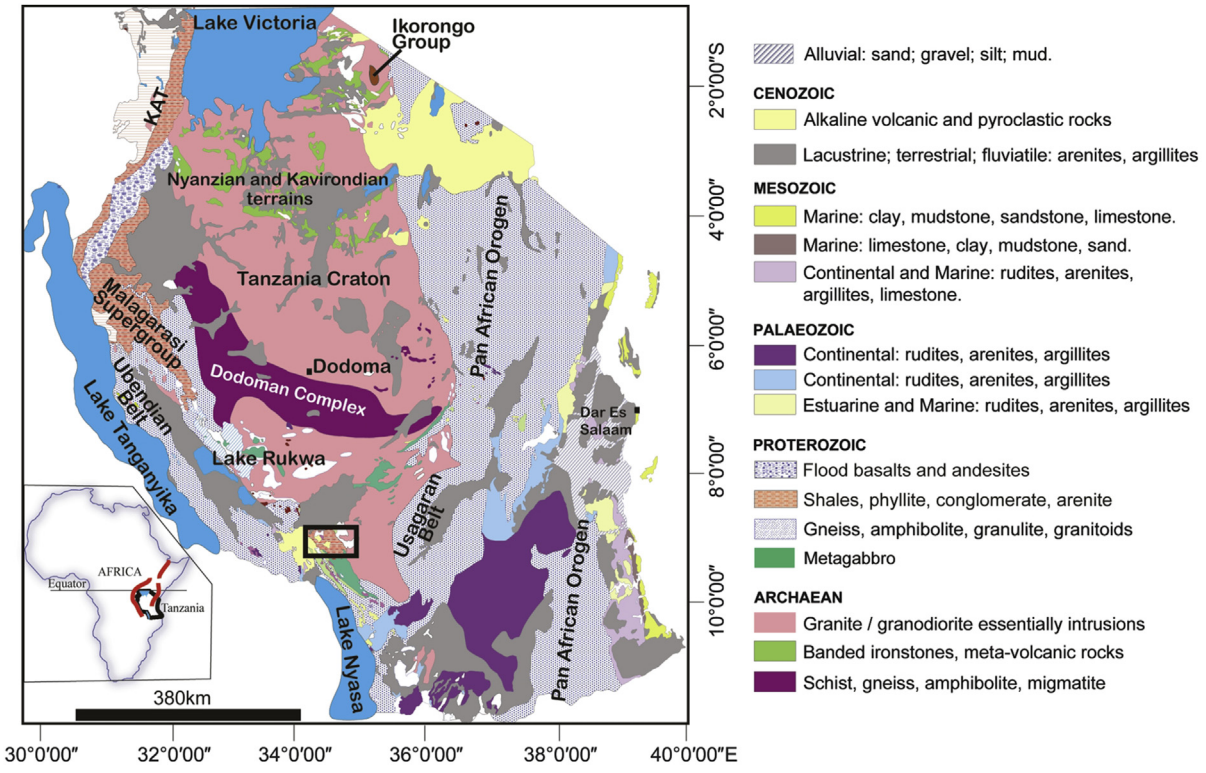


Figure 1. A regional geological map of Tanzania showing the various terrains. The geological setting of the Buanji basin is demarcated in the dark, solid square. The African map (bottom left) showing the geographical setting of Tanzania (map modified from Kasanzu et al., 2016b). KAT = Karagwe-Ankolean Terrain.

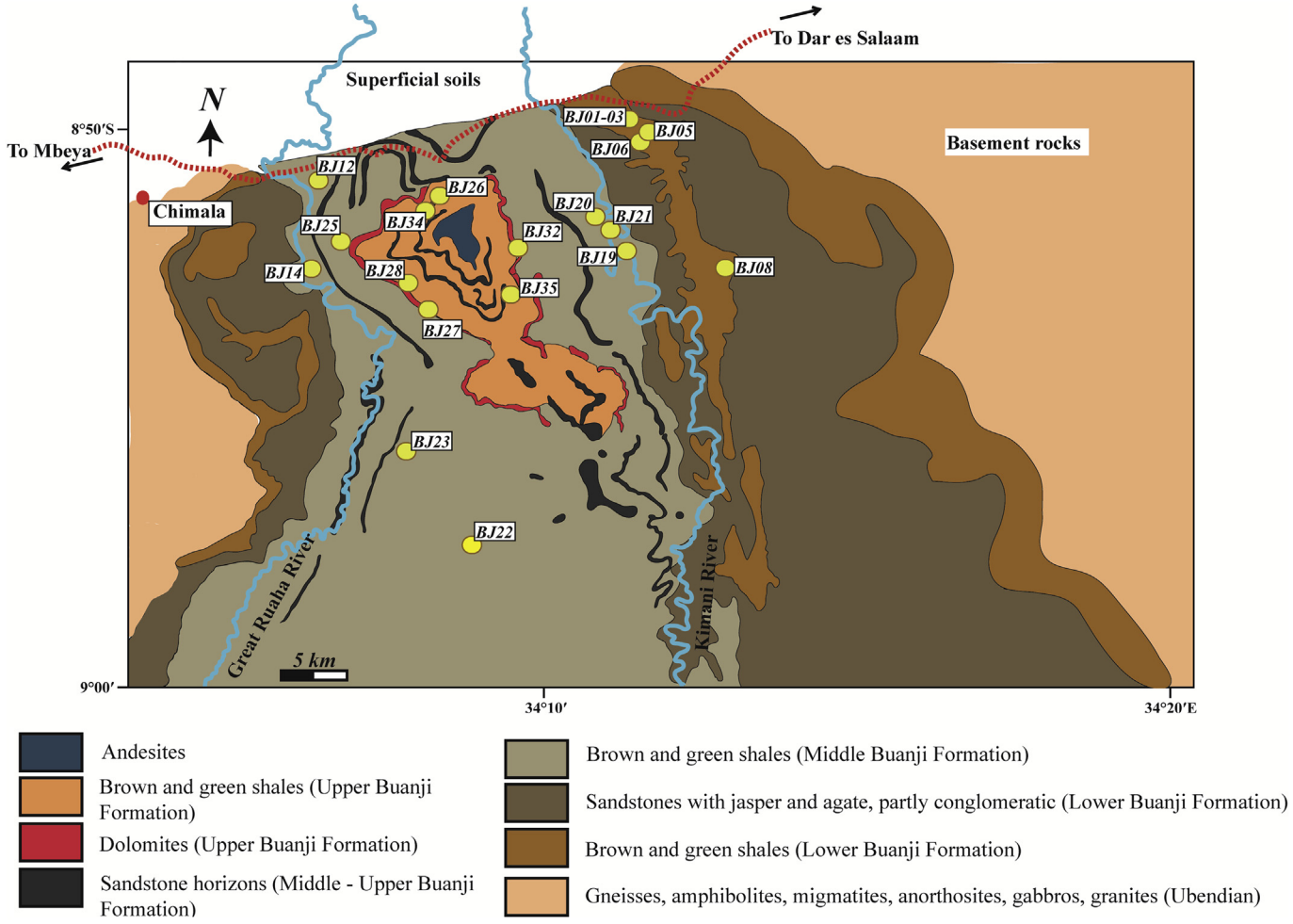


Figure 2. Geological map of the Buanji Group rocks showing the location of the samples used in this study (modified from Harpum and Brown, 1958). Yellow dots represent sampled locations.

brown and green shales with occasional cross-bedded quartzitic sandstones and conglomerates composed of pebbles of jasper and agate and reddish shales with occasional quartzitic sandstones (Fig. 3).

The middle Buanji Formation consists of cupriferous green shales that are intercalated with quartzitic sandstones and occasional conglomeratic horizons whose upper part comprises dolomites. In some places, the shales are micaceous and are usually interbedded with siltstones and quartzitic sandstones which are cross-bedded and contain ripple marks.

Thus, the upper Formation is composed largely of greenish, grayish or buff-coloured shales (Fig. 2), mudstones, dolomites, with intercalated sandstones and horizons of sandstones that also in some instances contain ripple marks and are cross-bedded. The upper Formation ends with effusive volcanism represented by highly vesicular lavas on Chaufukwe Mountain (Figs. 1–3). These lavas which are andesitic in composition erupted at 1674 ± 15 Ma (Manya, 2013) and are thus part of the late Paleoproterozoic magmatic events recorded in the Ubendian belt. The documented sedimentary structures in the basin and presence of dolomites in upper parts of the Group are suggestive of fluvial to lacustrine depositional environments on a continental setting.

3. Sampling and analytical methods

A total of 20 fresh samples were collected from the lower ($n = 6$), middle ($n = 8$) to upper ($n = 6$) Buanji formations of the stratigraphic column (Figs. 2 and 3). The samples were washed and oven-dried at 70 °C overnight at the Southern and Eastern Africa Mineral Centre (SEAMIC) Laboratories, Dar es Salaam, Tanzania. The dried samples were left to cool for 24 h. The samples were then pulverized in an agate planetary mill to <0.063 mm grain size, homogenized and packed into plastic bags. Five g aliquots of each powdered sample were packed and sent to the Activation Laboratories Ltd. of Ontario, Canada, for major, trace elements and Sm-Nd isotopic data determination. Major and trace elements analyses were performed using a Thermo Jarrell-Ash ENVIRO II Inductively Coupled Plasma Optical Emission Spectrometer (ICP-OES) and a Perkin Elmer SCIEX ELAN 6000 Inductively Coupled Plasma Mass Spectrometer (ICP-MS), respectively.

For ICP analyses, 0.25 g aliquots of each sample were mixed with a flux of lithium metaborate and lithium tetraborate and fused in an induction furnace. The molten melt was immediately poured into a solution of 5% HNO_3 containing an internal In standard, and was thoroughly mixed for ~30 minutes to achieve complete dissolution. An aliquot of the sample solution was

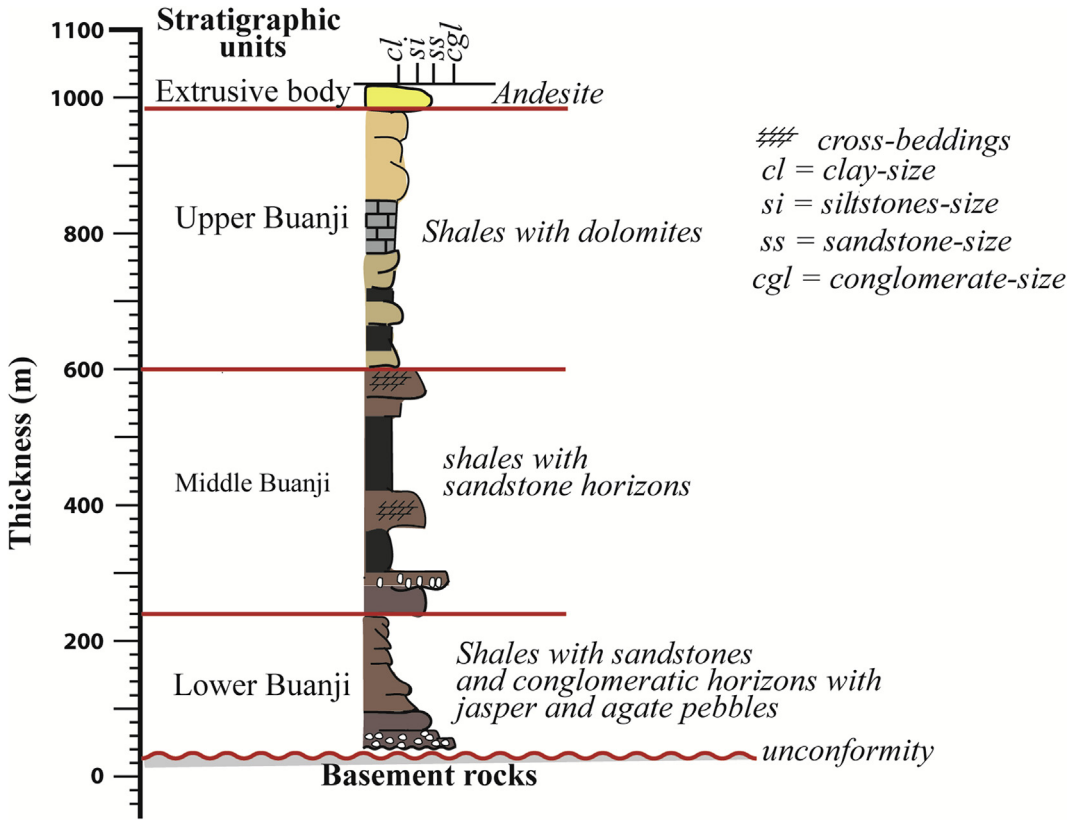


Figure 3. A stratigraphic section showing three formations sampled in the current study. All lithological details for each formation are indicated.

analysed for major oxides and the trace element Sc, on a combination sequential Thermo Jarrell-Ash ENVIRO II ICP-OES. Detection limits were 0.01 wt.% for all major elements and 2 ppm for Sc. Calibration was performed using seven USGS and Canmet certified reference materials. Loss on Ignition (LOI) was determined from the weight loss after roasting the samples at 1050 °C for 2 h. Totals ranged between 98.1 and 101 wt.% for major elements. The other aliquot of the sample solution was spiked with internal In and Rh standards to cover the entire mass range, and further diluted. Compared to the USGS W-2a standard, analytical errors for major elements were better than 3% (except for P_2O_5 which was 7%) and better than 8% for most trace elements.

Rock powders for Sm-Nd were dissolved in a mixture of HF, HNO_3 and $HClO_4$. Each sample was totally spiked with a $^{149}Sm/^{146}Nd$ mixed solution prior to decomposition. Sm and Nd were separated by extraction chromatography on HDEHP covered Teflon powder. Accuracy of the measurements of Sm, Nd contents is ±0.5%, $^{147}Sm/^{144}Nd = \pm 0.5\%$ (2σ). Analyses were performed on a Triton-MC mass-spectrometer at the Activation Laboratories.

4. Results

4.1. Major and trace elements composition

The major element compositions of the samples are compared to those of the post-Archaean Australian Shale (PAAS) of Taylor and McLennan (1985) and the average Proterozoic Shale (PS) of Condie (1993) which are regarded as modal composites representing the composition of post-Archaean upper continental crust (Roddaz et al., 2006; Kasanzu et al., 2008). The samples have SiO_2, TiO_2, Al_2O_3 and K_2O compositions that are similar to those of both PAAS and PS (Fig. 4). Fe_2O_3 and MnO contents in the lower Buanji are depleted relative to PAAS and PS whereas most middle Buanji samples show enrichments in MnO. The upper Buanji samples are either depleted or enriched in MnO contents. Compared to PAAS and PS, the contents of CaO, Na_2O and MgO are depleted for most samples (Fig. 4).

Shales from all the stratigraphic units of the Buanji Group show similar patterns in the primitive mantle normalized diagrams (Fig. 5). The elements Ba, Nb, Ta, Ce and Sr are depleted whereas Rb, La, Pb, Nd and Hf show enrichments relative to adjacent elements (Fig. 5). These contents are generally comparable to PAAS and PS with the exception of enrichments in Ba and substantial depletions in Sr, Pb and Zr (Fig. 6). The PS normalized diagrams also indicate an overall progressive increase of Cr, Co, Ni and V contents from the lower Buanji up-stratigraphy (Fig. 6).

The total REE contents for the lower Buanji shales range between 242 and 297 ppm with the exception of BJ08 which shows much lower contents (REE_{total} = 101 ppm; see Table 1). The depleted contents of the REE in BJ08 could be attributed to either quartz dilution and/or modest clay contents as evidenced by its lower Al_2O_3 composition (Table 1). Total REE compositions of the middle and upper Buanji samples are indistinguishable from those of the lower Buanji and are 220–289 ppm and 200–247 ppm, respectively.

Chondrite-normalized REE patterns for the lower Buanji (Fig. 7) reveal a PAAS-like feature with an enrichment of the LREE (mean $(La/Yb)_{CN}$ = 13; the subscript CN refers to chondrite-normalized

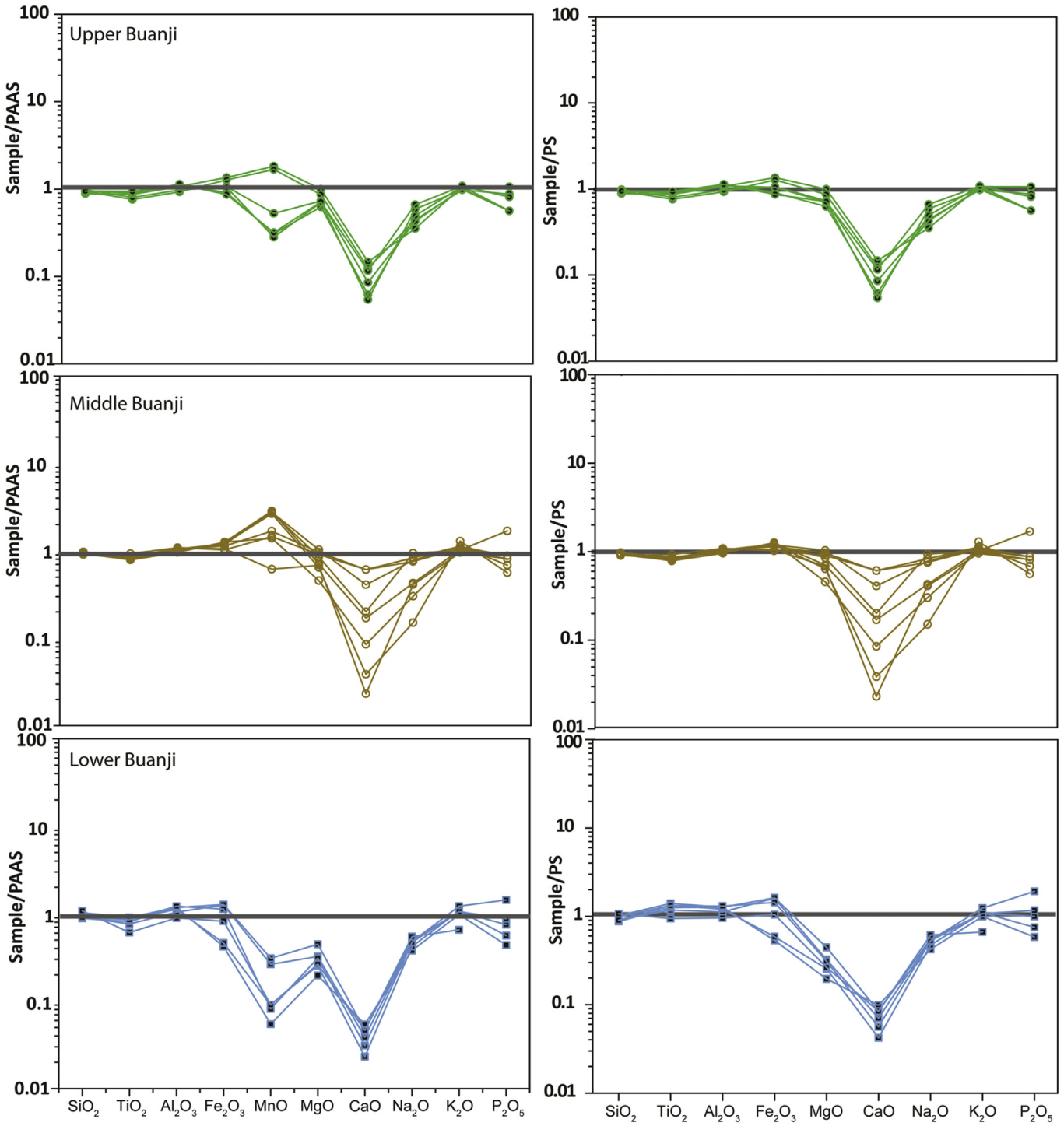


Figure 4. PAAS and PS normalized major oxide compositions for the Buanji samples. PAAS and PS data are from Taylor and McLennan (1985) and Condie (1993).

values) and flat HREE (mean $(Gd/Yb)_{CN} = 1.85$). Similarly, all the middle Buanji samples show an overall fractionated-concave-up pattern with enrichments in the LREE (mean $(La/Yb)_{CN} = \sim 12$) and relative flat HREE patterns (mean $(Gd/Yb)_{CN} = \sim 1.55$; see Fig. 7). Samples from the upper Buanji also reveal similar patterns with mean $(La/Yb)_{CN}$ and $(Gd/Yb)_{CN}$ values of 9.06 and 1.51, respectively. All the Buanji samples exhibit negative Eu anomalies ($Eu/Eu^* = 0.61–0.81$).

4.2. Sm-Nd isotopic data

The Sm and Nd contents as well as the Nd-isotopic compositions for selected samples from each stratigraphic unit are presented in Table 2. Nd-isotopic data from the lower Buanji yielded a depleted mantle model (T_{DM}) age of 2100 Ma and an $\varepsilon_{Nd(0)}$ value of −21.9. These values differ from those of the middle Buanji shales (T_{DM} age = 2486–2155 Ma, $\varepsilon_{Nd(0)} = -20.0$ to −19.4) as well as those of

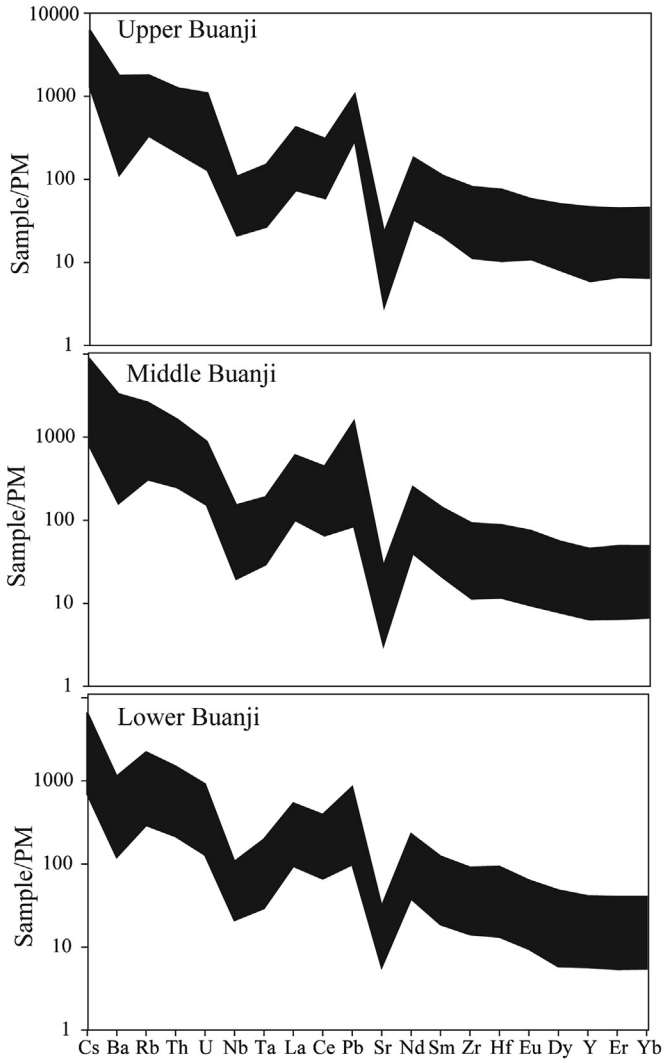


Figure 5. Primitive mantle (PM) normalized diagrams for the Buanji samples. Normalizing values are from Sun and McDonough (1989).

the upper Buanji (T_{DM} age = 2535–2379 Ma, $\varepsilon_{Nd(0)}$ = −19.5 to −18.7).

5. Discussion

5.1. Extent of paleo-weathering

The Chemical Index of Alteration (CIA) concept hinges on the chemical behaviour of various elements such as Ca, Na, K, and Al during silicate weathering at surface conditions (Nesbitt and Young, 1982). The major elements Ca, Na, and K are easily leached away from weathering profiles while elements such as Al are not easily affected by chemical weathering processes (Nesbitt and Young, 1984; Taylor and McLennan, 1985; Roddaz et al., 2006). This concept can be translated into absolute values and these can be interpreted in the context of weathering intensities. We have used this approach to constrain the extent of chemical weathering for the Buanji samples. We computed CIA indices using the equation developed by Nesbitt and Young (1982) as shown below;

$$\mathrm{CIA} = \left(\frac{\mathrm{Al_2O_3}}{\mathrm{Al_2O_3} + \mathrm{Na_2O} + \mathrm{CaO^*} + \mathrm{K_2O}}\right) \times 100$$

CaO* in this formula represents CaO in the silicate fraction and adopting the assumption of Bock et al. (1998), CaO contents in the equation were accepted only if CaO ≤ Na_2O. When CaO contents are higher than those for Na_2O, only the contents of the later were taken to substitute for anomalous CaO compositions in the samples. None of the samples were subjected to this correction (Table 1).

All samples (except two; see Fig. 8) from the lower Buanji Formation have their CIA values between 77 and 82 (mean = 81); a feature which is interpreted by Nesbitt and Young (1982) to imply extreme weathering (CIA = 80–100). CIA values obtained for these samples are suggestive of a highly weathered source in a warm, humid climate (Nesbitt and Young, 1982). CIA values for the middle Buanji samples are relatively lower (73–81; mean = 76) than those of the lower Buanji samples but are slightly higher than those of the upper Buanji (77–80; mean = 79). Despite trial disparity between the middle and upper Buanji samples, most samples represent a protolith that was exposed to intermediate weathering intensity (Fig. 8). This feature indicates that the source rocks of the middle and upper Buanji sediments were exposed to a warm, humid climate (Nesbitt and Young, 1982).

In Fig. 9, we assess the weathering trends of our samples using triangular plots developed by Englund and JØrensen (1973). According to Englund and JØrensen (1973), un-weathered rocks plot in field A-II of Fig. 9 whereas increasing chemical weathering moves the samples through fields A-III or B-III, A-IV, B-IV and when all mobile elements are leached away the samples plot into field C-IV. This trend can be represented mathematically as shown below;

$$\mathrm{M1} = (\mathrm{FeO} + \mathrm{MgO} + \mathrm{Al_2O_3})/(\mathrm{K_2O} + \mathrm{CaO} + \mathrm{Na_2O})$$

$$\mathrm{M2} = \mathrm{Al_2O_3}/(\mathrm{FeO} + \mathrm{MgO})$$

As shown in Fig. 9, the lower Buanji samples scatter between fields A II-III, A-VI and B-IV with two samples plotting in the extremely weathering region (field C-IV) whereas the middle Buanji samples cluster between A-III and A-IV fields. Most green shale samples from the upper Buanji are enclosed in field A-IV, attesting to a more weathered precursor than that for the middle Buanji, but relatively lower than for lower Buanji (Fig. 9). These observations further corroborate the conclusions based on CIA values of mainly warm, humid climatic conditions prevailing during the deposition of the Buanji rocks. However, we do not discount the role of other factors such as orography that can have an influence on weathering intensities.

5.2. Nature of the detrital protolith and paleo-tectonic setting

Ratios of the relative immobile elemental pairs Th/Sc, La/Sc, La/Th, Co/Th and Cr/Th are useful for provenance determination of fine grained sediments as such elements are not fractionated during surface processes (Basu et al., 1990; Chakrabarti et al., 2007). Kasanzu et al. (2008) showed that the trace elements La and Th are enriched in felsic protoliths and are therefore depleted in basic rocks whereas Sc, Co and Cr show the opposite trend. When compared with PAAS and PS, the Th/Sc, La/Sc, La/Th, Co/Th and Cr/Th ratios for lower and middle Buanji rocks generally indicate a more felsic parentage than that for PAAS and PS (Table 3). The overlapping Th/Sc, La/Sc and Co/Th ratios for upper Buanji samples, relative to PAAS and PS, suggests that the upper Buanji rocks were derived from a source compositionally similar to that of both PAAS and PS.

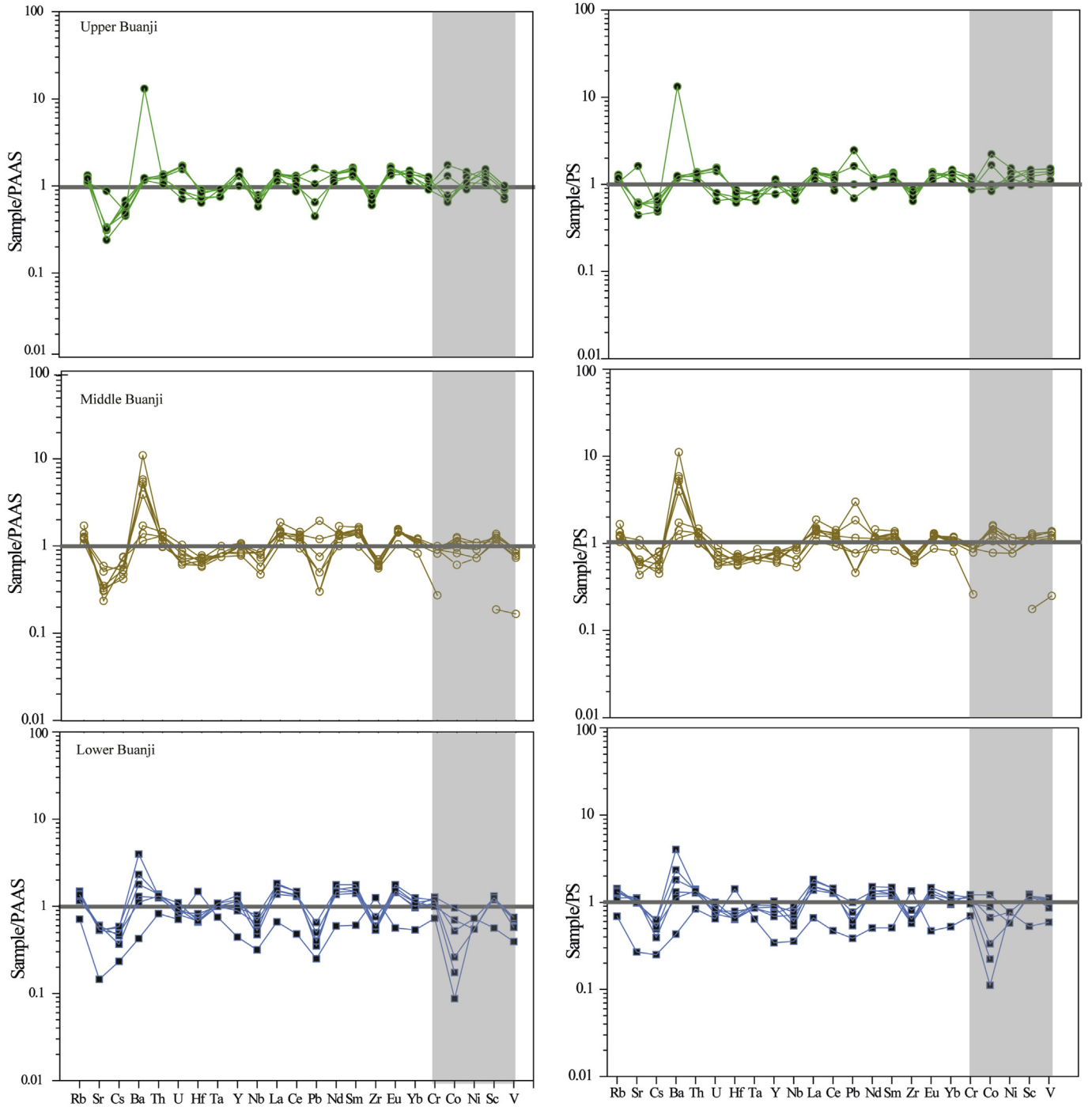


Figure 6. PAAS and PS-normalized diagrams for rocks from Buanji Group rocks. PAAS and PS normalizing values are from Taylor and McLennan (1985) and Condie (1993), respectively.

When compared to the average Th/Sc and La/Sc ratios of sediments derived from felsic and basic rocks (Table 3), the lower Buanji samples further suggest a more felsic character than samples from both the middle and upper Buanji. Similarly, samples from the middle and upper Buanji suggest derivation from felsic rocks but this character decreases up-stratigraphy relative to the basal lower Buanji samples. Thus, the overall felsic magnitude is of the order: lower Buanji > middle Buanji > upper Buanji. This trend is also apparent in the PAAS and PS normalized trace element diagrams in Fig. 6 whereby the transition trace elements Cr, Co, Ni, Sc and V progressively increase up-stratigraphy.

The REE contents can help unravel the nature of source rocks as their patterns are preserved in clastic sedimentary rocks during weathering, erosion and lithification (Taylor and McLennan, 1985). Unlike mafic sources, felsic sources are rich in the LREE and are characterised by negative Eu anomalies (Ali

Table 1
Major (wt.%) and trace (ppm) element contents of rock samples from Buanji Group.

	Lower Buanji						Middle Buanji								Upper Buanji					
	BJ01	BJ02	BJ03	BJ05	BJ06	BJ08	BJ12	BJ14	BJ19	BJ20	BJ21	BJ22	BJ23	BJ25	BJ26	BJ27	BJ28	BJ32	BJ34	BJ35
SiO_2	64.18	57.21	62.31	55.26	56.91	67.46	56.62	57.01	57.03	57.57	59.26	57.99	58.92	60.69	55.4	58.88	61.45	57.96	59.15	59.19
Al_2O_3	22.23	19.6	21.12	22.13	22.84	16.79	20.41	20.37	18.53	19.76	19.14	19.64	18.06	18.23	20.13	17.44	18.34	21.33	20.44	21.28
Fe_2O_3	3.01	9.03	3.32	9.14	8.12	5.9	7.56	7.36	8.57	8.15	8.57	8.71	9.03	9.05	9.76	9.17	7.63	6.5	7.5	6.22
MnO	0.006	0.029	0.01	0.034	0.009	0.01	0.068	0.16	0.303	0.185	0.301	0.292	0.313	0.153	0.201	0.185	0.058	0.034	0.031	0.035
MgO	0.43	0.71	0.56	0.98	0.68	0.58	1.5	1.99	2.26	2.11	1.87	1.41	1.55	1	2.18	1.89	1.6	1.37	1.54	1.56
CaO	0.07	0.05	0.03	0.06	0.04	0.06	0.03	0.79	0.53	0.79	0.26	0.05	0.22	0.11	0.19	0.16	0.11	0.08	0.07	0.15
Na_2O	0.45	0.57	0.5	0.59	0.56	0.65	0.49	0.99	0.93	0.9	1.12	0.18	0.51	0.36	0.42	0.53	0.51	0.59	0.7	0.79
K_2O	3.61	4.49	3.97	3.89	3.89	2.41	3.52	4.15	4.12	3.93	3.7	4.75	3.8	3.77	3.92	3.61	3.71	3.95	3.65	4
TiO_2	0.894	0.755	0.847	0.804	0.846	0.604	0.92	0.818	0.842	0.789	0.852	0.788	0.78	0.858	0.861	0.753	0.794	0.914	0.89	0.929
P_2O_5	0.07	0.23	0.09	0.12	0.14	nil	0.13	0.11	0.14	0.14	0.13	0.09	0.14	0.27	0.17	0.14	0.09	0.09	0.09	0.13
LOI	5.26	6.47	5.63	5.96	6.2	5.69	7.12	5.95	6.14	5.86	5.07	6.23	6.04	5.61	7.1	5.91	6.44	7.25	6.82	6.31
Total	100.2	99.15	98.39	98.97	100.2	100.2	98.36	99.7	99.4	100.2	100.3	100.1	99.36	100.1	100.3	98.67	100.7	100.1	100.9	100.6
CIA	82	77	80	81	81	82	81	73	73	73	75	78	77	79	79	77	78	80	80	78
Sc	19	21	20	20	20	9	19	22	22	21	18	20	18	18	21	19	17	25	23	25
V	105	86	108	106	112	59	123	135	136	133	110	138	116	116	134	105	112	149	140	152
Ba	845	2588	1161	1505	723	277	1112	805	901	744	3554	2533	7143	3770	789	8514	754	774	760	801
Sr	121	107	120	106	107	29	66	60	62	62	102	47	118	61	62	175	48	64	67	65
Y	26	31	36	24	32	12	29	26	28	28	22	23	29	27	27	35	39	40	35	35
Zr	159	113	123	112	125	264	127	122	125	123	129	139	148	123	126	144	143	163	171	162
Cr	120	110	130	140	130	80	100	110	110	100	90	110	100	100	100	110	100	140	130	140
Co	4	16	6	22	12	2	19	18	25	22	28	26	29	14	30	40	16	15	18	15
Ni	nil	30	30	40	40	40	40	50	50	50	50	60	60	40	50	80	60	70	60	60
Rb	186	238	209	225	217	114	196	218	222	203	192	274	199	204	212	174	179	199	182	195
Nb	15	9	10	12	13	6	14	11	16	11	16	16	11	15	15	11	11	14	13	13
Cs	5.5	8.5	6.9	8.8	7.3	3.5	6.3	11.9	11.3	11.1	9.1	9.2	7.9	7.1	10.2	7.6	6.8	8.6	7.2	9.1
La	66.8	57.3	69.3	52.3	57.9	25.2	71	52.3	53.2	53.8	52.2	55.2	47.2	57	52.3	51.7	49.9	53.7	51.1	43.1
Ce	118	106	118	104	108	38.5	116	103	108	107	99.4	103	94.8	84	105	98.8	69.2	100	93.1	81.1
Pr	14.3	13.5	15.7	11.8	12.9	5.34	15.3	11.4	12	11.8	11.4	12.2	10.4	11.6	11.8	11.4	10.8	11.6	10.6	9.15
Nd	51.8	49.8	56.6	43.7	46.8	19	54.1	43.4	44.3	43.6	42.6	43.9	38.6	41.6	44.3	43.3	43.3	43.3	38.2	35.4
Sm	8.3	9.3	9.9	7.9	8.3	3.4	9.2	7.7	8.8	8.5	7.7	8	7.7	7.6	9.1	8.7	8.3	8.4	7.2	7.4
Eu	1.59	1.81	1.94	1.58	1.65	0.62	1.58	1.5	1.6	1.57	1.62	1.68	1.67	1.72	1.83	1.78	1.63	1.57	1.46	1.48
Gd	6	7.9	8.5	7	7.3	2.6	6.8	5.5	6.1	6.3	4.9	5.8	6.7	5.5	7.7	7.7	8	6.6	6	6
Tb	0.8	1.2	1.2	1	1	0.4	1	0.9	1	1	0.8	0.9	1	0.9	1.1	1.2	1.1	1.1	1	1.1
Dy	4.3	6.2	6.5	5.4	5.7	2.4	5.7	5.1	5.5	5.8	4.4	5.2	5.3	5.3	5.9	6.8	6	6.2	6	6.3
Ho	0.8	1.2	1.2	1	1	0.5	1.1	1	1.1	1.1	0.9	1	1.1	1	1.1	1.3	1.2	1.3	1.2	1.2
Er	2.6	3.2	3.6	2.8	3	1.3	3.1	2.9	3.3	3.1	2.6	2.8	3.2	3.2	3.2	3.7	3.5	3.9	3.7	3.6
Tm	0.41	0.47	0.56	0.44	0.46	0.2	0.51	0.46	0.53	0.49	0.42	0.45	0.47	0.46	0.51	0.55	0.56	0.63	0.61	0.57
Yb	2.7	3.1	3.5	2.8	3.1	1.5	3.3	3.2	3.4	3.3	2.9	2.9	3.1	3	3.2	3.7	3.8	4.2	3.9	3.8
Lu	0.39	0.47	0.5	0.41	0.48	0.24	0.48	0.44	0.52	0.5	0.42	0.44	0.48	0.47	0.51	0.53	0.62	0.6	0.57	0.6
Hf	4.1	3.4	3.7	3.3	3.4	7.4	3.6	3.4	3.4	3.2	3	3.4	3.9	2.9	3.2	3.6	3.7	4.1	4.5	4.2
Ta	1.2	1.2	1.3	1.2	1.3	0.9	1.2	1	0.9	1	1	1	0.9	0.9	1.1	0.9	0.9	1.1	1.1	1.1
Pb	7	13	7	10	8	5	6	10	24	39	15	6	nil	10	21	nil	nil	32	9	13
Th	18.3	19.2	20.1	19.5	19.2	12	21.1	18.8	18.7	19.2	18.3	16.6	16.4	14.2	17.6	15.9	15.3	19.8	18.6	19.2
U	2.7	2.5	2.9	2.9	3.4	2.2	3.2	2.6	2.5	2.7	1.9	1.9	2	2.2	2.7	2.2	2.7	5.3	4.8	5.2
Th/Sc	0.96	0.91	1.01	0.98	0.96	1.33	1.11	0.85	0.85	0.91	1.02	0.83	0.91	0.79	0.84	0.84	0.90	0.79	0.81	0.77
La/Sc	3.52	2.73	3.47	2.62	2.90	2.80	3.74	2.38	2.42	2.56	2.90	2.76	2.62	3.17	2.49	2.72	2.94	2.15	2.22	1.72
Zr/Sc	8.37	5.38	6.15	5.60	6.25	29.33	6.68	5.55	5.68	5.86	7.17	6.95	8.22	6.83	6.00	7.58	8.41	6.52	7.43	6.48
La/Th	3.65	2.98	3.45	2.68	3.02	2.10	3.36	2.78	2.84	2.80	2.85	3.33	2.88	4.01	2.97	3.25	3.26	2.71	2.75	2.24
Co/Th	0.22	0.83	0.30	1.13	0.63	0.17	0.90	0.96	1.34	1.15	1.53	1.57	1.77	0.99	1.70	2.52	1.05	0.76	0.97	0.78
Cr/Th	6.56	5.73	6.47	7.18	6.77	6.67	4.74	5.85	5.88	5.21	4.92	6.63	6.10	7.04	5.68	6.92	6.54	7.07	6.99	7.29
Nb/Ta	12.50	7.50	7.69	10.00	10.00	6.67	11.67	11.00	17.78	11.00	16.00	16.00	12.22	16.67	13.64	12.22	12.22	12.73	11.82	11.82
Zr/Sm	19.16	12.15	12.42	14.18	15.06	77.65	13.80	15.84	14.20	14.47	16.75	17.38	19.22	16.18	13.85	16.55	17.23	19.40	23.75	21.89
Ce/Pb	16.86	8.15	16.86	10.40	13.50	7.70	19.33	10.30	4.50	2.74	6.63	17.17	0.00	8.40	5.00	0.00	0.00	3.13	10.34	6.24
$(La/Yb)_{CN}$	16.68	12.46	13.35	12.59	12.59	11.33	14.51	11.84	10.55	10.99	12.14	12.83	10.27	12.81	11.02	9.42	8.85	8.62	8.83	7.65
$(Gd/Yb)_{CN}$	1.79	2.05	1.96	2.02	1.9	1.39	1.66	1.61	1.44	1.54	1.36	1.61	1.74	1.47	1.94	1.68	1.69	1.27	1.24	1.27
Eu/Eu*	0.68	0.65	0.65	0.65	0.65	0.64	0.61	0.69	0.66	0.61	0.80	0.75	0.71	0.81	0.67	0.66	0.61	0.65	0.68	0.68

et al., 2014). REE plots (Fig. 7) for all the three Buanji formations are characterised by enrichments in LREE relative to the HREE and have negative Eu anomalies. This observation further supports the inference of an overall felsic provenance for the Buanji rocks.

The Sm-Nd systematics are vital in provenance studies as the sediments record and preserve age information about source rocks (e.g., Chakrabarti et al., 2007; Ali et al., 2014). For instance, a increase in εNd or an decrease in T_{DM} in sediments may indicate a juvenile protolith or termination of older crustal provenance (Chakrabarti et al., 2007; Fuenlabrada et al., 2010). The lower Buanji rocks are characterised by a lower T_{DM} age and a relatively higher ε_{Nd} value (2100 Ma, −21.9 respectively) relative to the overlying middle (2486–2155 Ma, −19.4 to −20.0) and upper Buanji (2535–2379 Ma, −18.7 to −19.5). The T_{DM} age of the lower Buanji sample suggests derivation of its detritus from a source terrane with a mean Eburnean mantle extraction age, which corresponds to the Ubendian terrain. The overlapping T_{DM} ages between the middle and upper Buanji suggest multiple sources involving the Archaean cratonic rocks mixing with the Ubendian.

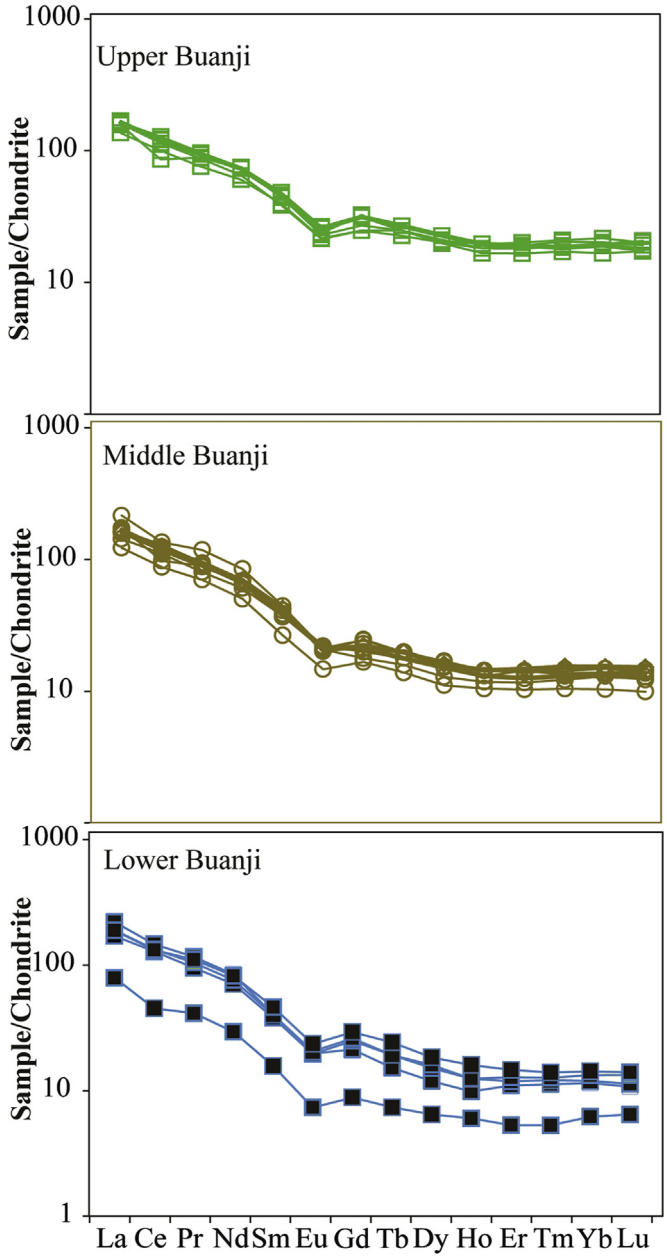


Figure 7. Chondrite normalized REE patters of the Buanji samples. Normalizing values are from Sun and McDonough (1989).

However, the average T_{DM} ages and lower ε_{Nd} for the upper Buanji suggests that much of the detritus was sourced from the craton from north of the basin. The middle Buanji could have sampled a more diverse protolith, given the relatively larger spread in the T_{DM} ages. These temporal variations in the Sm-Nd character of source rocks point to drainage shifts during the Precambrian (see Figs. 10 and 11). In this view, the deposition of all Buanji formations indicates topographic decay of the Ubendian during orogenesis *sensu* denudation in the realm of Columbia supercontinent evolution.

The plots of Nb/Ta versus Zr/Sm and Ce/Pb versus Ce are useful proxies for ancient tectonic settings discrimination (Chakrabarti et al., 2007). The discriminatory plots shown in Fig. 12a indicate that the paleo-tectonic setting of the sources for the Buanji rocks was largely a subduction zone akin to that generating Island Arc Basalts (IAB). This feature is also reflected in the plot of Ce/Pb versus Ce (Fig. 12b) where most of the Buanji rocks plot in the global arcs setting which implies mixing of primitive mantle and continental crust detritus (Foley et al., 2002). These observations suggest that the Buanji basin was located near an arc system during the Precambrian in the course of the amalgamation of the Columbia supercontinent, consistent with an extensional continental backarc basin (Busby and Azor, 2012). Additionally, the considerable depletions in Ba, Nb, Ta, Sr and the significant enrichments in Rb, Th, Ce, Nd and Pb observed in the primitive mantle normalized diagram (Fig. 5) support an arc setting for the provenance rocks (Chakrabarti et al., 2007). This is in agreement with the work of Boniface et al. (2012), Manya (2013, 2014) and Kazimoto et al. (2015) who all suggested that most rocks in the Ubendian belt formed in a Paleoproterozoic arc setting.

6. Summary and conclusions

Major and trace element compositions and Nd-isotopic data for the ~1.67 Ga clastic sedimentary rocks of the Buanji Group reveal the following:

(1) The Buanji Group shales are generally comparable to PAAS and PS in terms of their major and trace element compositions and are interpreted to have been derived from continental felsic sources.
(2) The Chemical Indices of Alteration (CIA) for the lower (81), middle (76) and upper Buanji (79) generally indicate intermediate to extreme chemical weathering of the source rocks. These features are suggestive of warm, humid climatic conditions during the late Paleoproterozoic in the region.
(3) The provenance ratios (Th/Sc, La/Sc, La/Th, Co/Th and Cr/Th), coupled with increasing concentrations in Cr, Ni, Co and V from the lower to upper Buanji formations are indicative of a decreasing felsic character up-stratigraphy and may suggest changes in sediment sources which may be attributed to paleodrainage shifts.
(4) The Nd mantle depleted model age for the lower Buanji Formation (T_{DM} = ~2100 Ma) suggest that the detritus were derived from an Eburnean crust which is consistent with the Ubendian rocks. T_{DM} ages of 2486–2155 Ma and 2535–2379 Ma, from the middle and upper Buanji formations,

Table 2
Sm-Nd isotopic data for the Buanji Group shales.

Samples	Formation	Sm (ppm)	Nd (ppm)	$^{147}Sm/^{144}Nd$	$^{143}Nd/^{144}Nd$	±2s	$f_{Sm/Nd}$	$\varepsilon_{Nd}(0)$	T_{DM} (Ma)
BJ15	Lower	9.78	62.47	0.09465	0.511514	2.0E−05	−0.51881	−21.9	2100
BJ23	Middle	7.7	39.04	0.11921	0.511611	2.0E−05	−0.39395	−20	2486
BJ25	Middle	7.01	39.66	0.1069	0.511644	8.0E−06	−0.45653	−19.4	2155
BJ35	Upper	7.07	34.87	0.12264	0.511638	2.0E−05	−0.37651	−19.5	2535
BJ27	Upper	9.22	46.79	0.11914	0.511677	7.0E−06	−0.39431	−18.7	2379

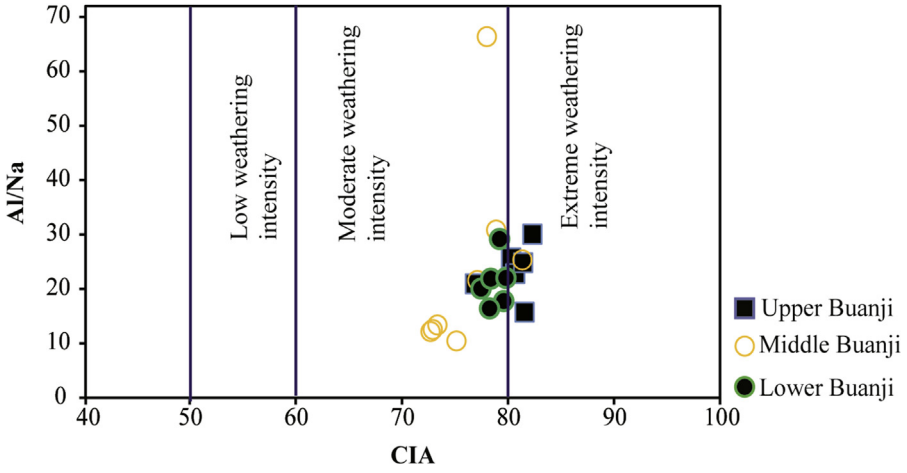


Figure 8. A binary plot of CIA versus Al/Na ratios for Buanji rocks. Note that most samples straddle the field between intermediate to extreme weathering intensities (demarcation fields are from Kasanzu et al., 2008).

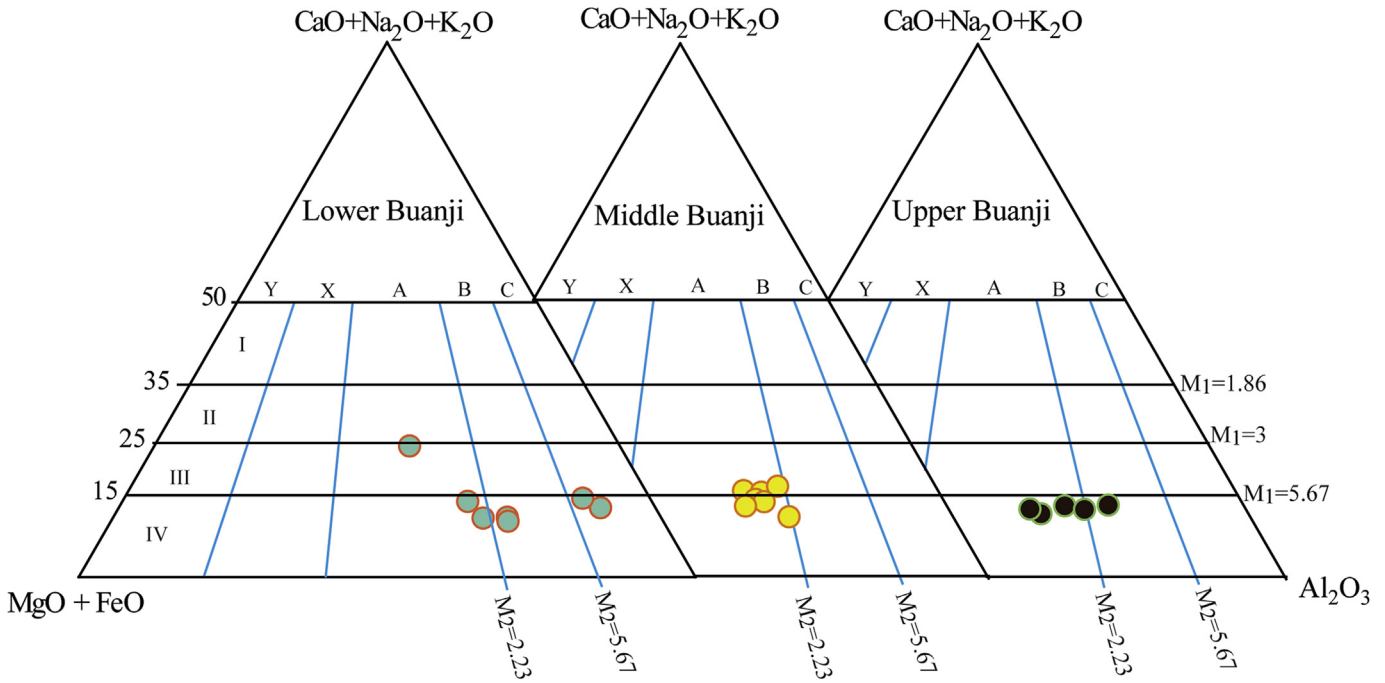


Figure 9. Weathering trends diagram adopted from Englund and Jørgensen (1973). The diagram illustrates that gradual increase in weathering (from un-weathered source) resulting in the loss of Ca, Na and K which is accompanied by an increase in M1 values (fields I to IV). An increase of M2 values (fields A IV to C IV) is a feature for extreme weathering. Note the varying degrees of chemical weathering for all samples from the three stratigraphic units of the Buanji Group. It is evident from the diagram that the magnitude of weathering is in the order of: lower Buanji > upper Buanji > middle Buanji.

Table 3
Provenance ratios for Buanji samples compared to established data from various lithologies.

Lithology	Th/Sc	La/Sc	La/Th	Co/Th	Cr/Th
Sands from felsic sources	20–0.83	2.5–16	–	0.22–1.5	0.5–7.7
Sands from basic sources	0.05–0.04	0.44–1.1	–	7.1–8.3	22–100
PAAS	0.78	2.38	2.66	1.59	7.94
PS	0.84	2.24	2.6	1.25	8.04
Lower Buanji	1.03	3	2.98	0.55	6.56
Middle Buanji	0.92	2.81	3.11	1.41	5.85
Upper Buanji	0.82	2.37	2.86	1.29	6.75

Note: Data for sands from felsic and mafic sources are from Taylor and McLennan (1985).

respectively; suggest a progressively increase of input from the Archaean Tanzania craton up-stratigraphy.

(5) The Nb/Ta, Zr/Sm and Ce/Pb data for the shales of the Buanji Group coupled with the negative anomalies in Nb and Ta in primitive mantle normalized diagrams indicate that the paleo-tectonic setting of the sources for the Buanji rocks was largely a subduction zone akin to that generating Island Arc Basalts (IAB). Thus, it is suggested that the Buanji's palaeogeography is consistent with an extensional continental backarc basin during the late Paleoproterozoic.

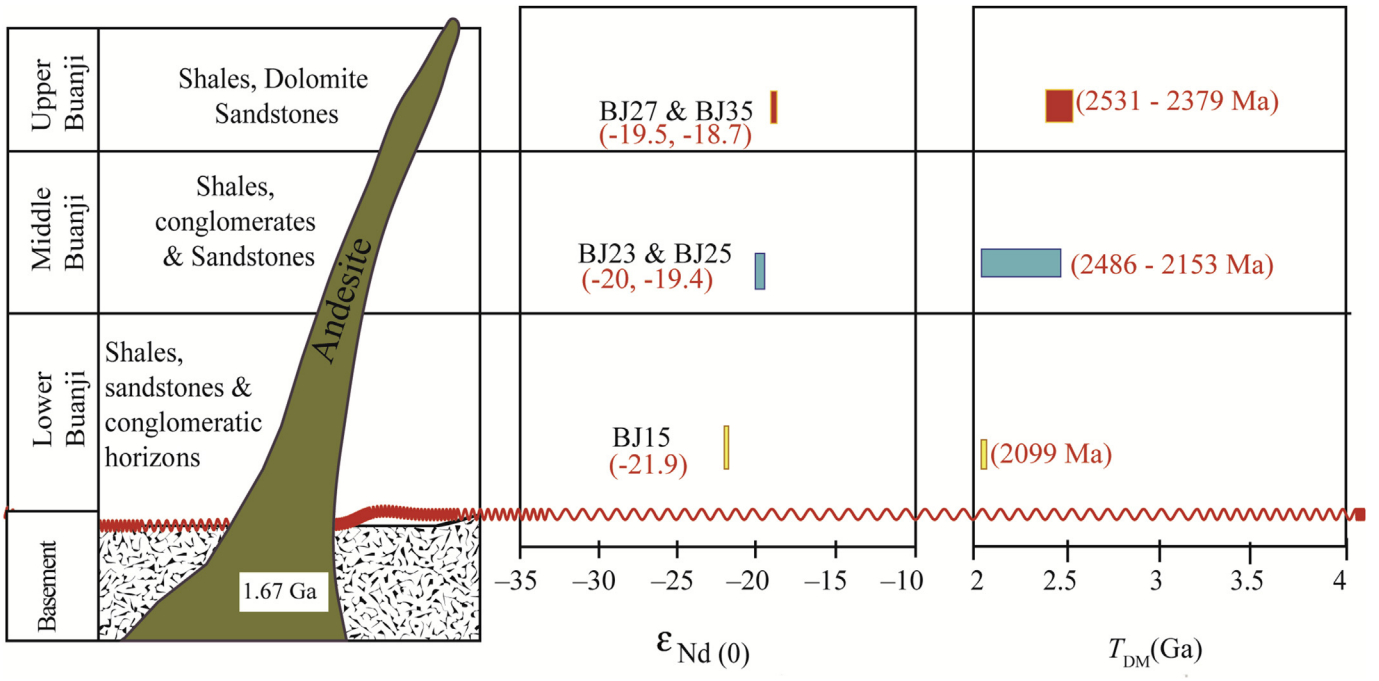


Figure 10. Sm-Nd systematics for the Buanji rocks. These data indicate a restricted source (Eburnean) for lower Buanji with a diversification of sources during deposition of the middle Buanji rocks. The upper Buanji Formation requires a more Archaean hinterland with a minor Eburnean source. The cartoon to the left shows the stratigraphic framework of the study area.

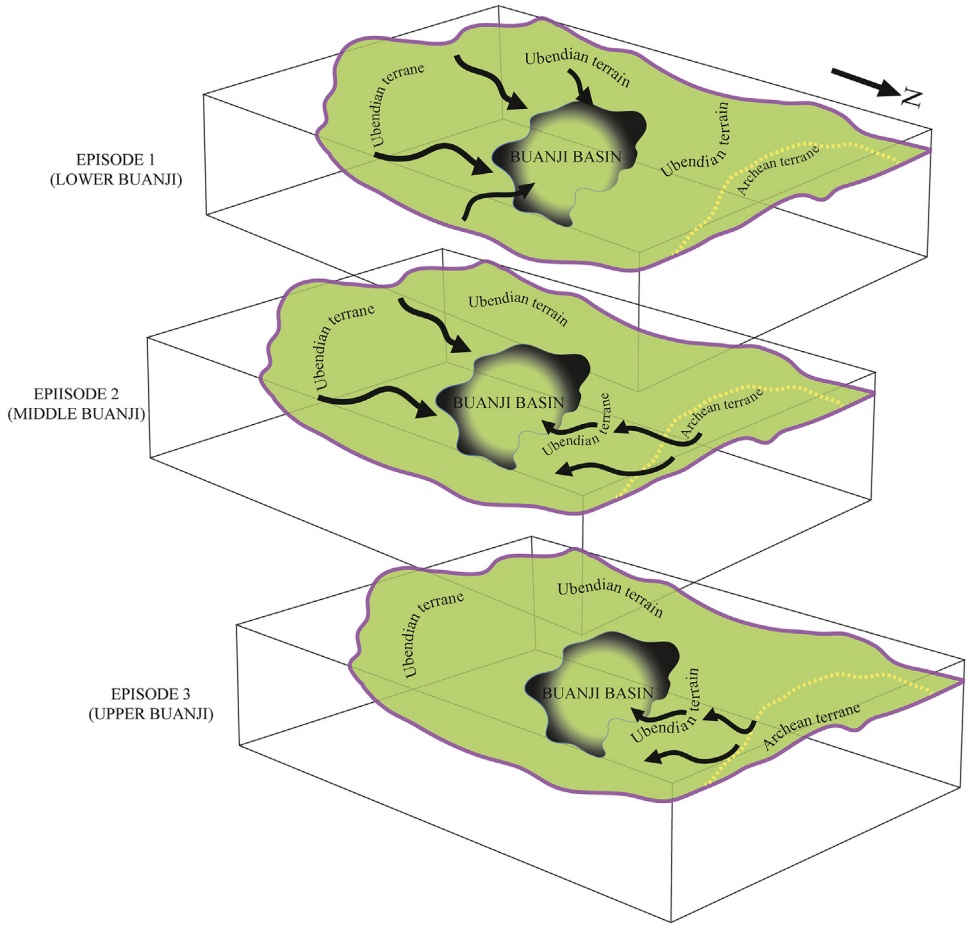


Figure 11. A cartoon (not to scale) showing possible sources of sediments that were deposited in the Buanji basin (sketched in grey) during the Precambrian. Episodes 1, 2 and 3 are the drainage scenarios during deposition of the lower, middle and upper Buanji, respectively.

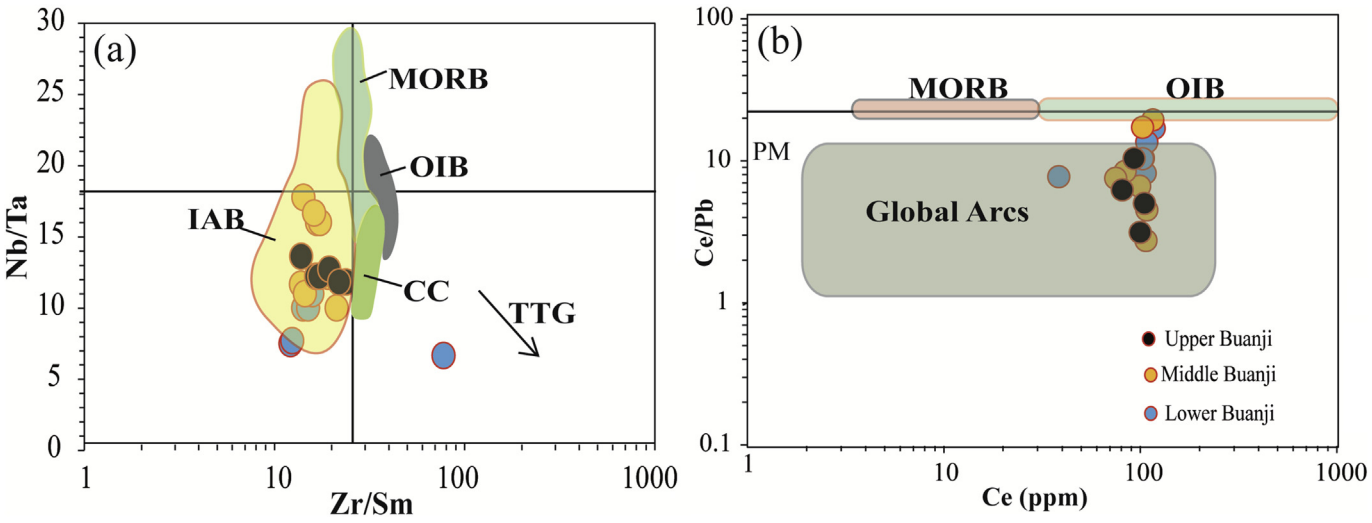


Figure 12. (a) A plot of Nb/Ta versus Zr/Sm ratios for the Buanji shales indicating the nature of the tectonic setting for the protolith. (b) A binary plot of Ce versus Ce/Pb for the Buanji shales indicating paleo-tectonic setting of samples in the basin. IAB = Island Arc Basalts; CC = Continental Crust; OIB = Oceanic Island Basalts.

Acknowledgements

We acknowledge the financial assistance we received from the Swedish International Development Agency (Sida) (Contribution No. 75000515) through the "Geology and mineralization of the Precambrian volcanic and associated plutonic rocks of SW Tanzania" project under the Earth Science Programme of CoNAS, University of Dar es Salaam (2009–2013 extended to June 2015). This assistance enabled us to conduct fieldwork in southwestern Tanzania as well as acquire the geochemical and isotopic data.

References

Ali, S., Statteger, K., Garbe-Schonberg, D., Frank, M., Kraft, S., Kuhnt, W., 2014. The provenance of Cretaceous sediments in the Tarfaya basin, SW Morocco: evidence from trace element geochemistry and radiogenic Nd-Sr isotopes. Journal of African Earth Sciences 90, 64–76.

Bahame, G., Manya, S., Maboko, M.A.H., 2016. Age and geochemistry of coeval felsic volcanism and plutonism in the Paleoproterozoic Ndembera Group of southwestern Tanzania: constraints from SHRIMP U-Pb and Sm-Nd data. Precambrian Research 272, 115–132.

Basu, A.R., Sharma, M., DeCelles, P.G., 1990. Nd, Sr-isotopic provenance and trace element geochemistry of Amazonian Foreland Basin Fluvial Sands, Bolivia and Peru: implications for Ensialic Andean Orogeny. Earth and Planetary Science Letters 105, 149–169.

Bock, B., McLennan, S.M., Hanson, G.N., 1998. Geochemistry and provenance of the middle Ordovician Austin Glen Member (Normanskill Formation) and the Taconian Orogeny in New England. Sedimentology 45, 635–655.

Boniface, N., Schenk, V., Appel, P., 2012. Paleoproterozoic eclogites of MORB-type chemistry and three Proterozoic orogenic cycles in the Ubendian Belt (Tanzania): evidence from monazite and zircon geochronology, and geochemistry. Precambrian Research 192–195, 16–33.

Boven, A., Theunissen, K., Sklyarov, E., Klerkx, J., Mel-nikov, A., Mruma, A., Punzalan, L., 1999. Timing of exhumation of a high-pressure mafic granulite terrane of the Paleoproterozoic Ubende Belt (west Tanzania). Precambrian Research 93, 119–137.

Busby, C., Azor, A., 2012. Tectonics of Sedimentary Basins. Wiley-Blackwell, 67pp.

Chakrabarti, R., Basu, A.R., Chakrabarti, A., 2007. Trace element and Nd-isotopic evidence for sediment sources in the mid-Proterozoic Vindhyan Basin, central India. Precambrian Research 159, 260–274.

Chen, M., Sun, M., Cai, K., Buslov, M.M., Zhao, G., Rubanova, E.S., 2014. Geochemical study of the Cambrian-Ordovician meta-sedimentary rocks from the northern Altai-Mongolian terrane, north-western Central Asian Orogenic Belt: implications on the provenance and tectonic setting. Journal of Asian Earth Sciences 96, 69–83.

Condie, K.C., 1993. Chemical composition and evolution of the upper continental crust: contrasting results from surface samples and shales. Chemical Geology 104, 1–37.

DaPeng, L., Chen, Y.L., Zhong, W., Yu, L., Zhou, J., 2011. Paleozoic sedimentary record of the Xing-Meng Orogenic Belt, inner Mongolia: implications for the provenances and tectonic evolution of the central Asian Orogenic Belt. Chinese Science Bulletin 57, 776–785.

Englund, J.-O., JØrgensen, P., 1973. A chemical classification system for argillaceous sediments and factors affecting their composition. Geologiska Foreningens i Stockholm Forhandlingar 286, 1–60.

Feng, R., Kerrich, R., 1990. Geochemistry of fine-grained clastic sediments in the Archean Abitibi Greenstone Belt, Canada: implications for provenance and tectonic setting. Geochimica et Cosmochimica Acta 54, 1061–1108.

Foley, S., Tiepolo, M., Vannucci, R., 2002. Growth of early continental crust controlled by melting of amphibolite in subduction zones. Nature 417, 837–840.

Fuenlabrada, J.M., Arenas, R., Fernandez, R.D., Martinez, S.S., Abati, J., Carmona, A.L., 2010. Sm-Nd isotope geochemistry and tectonic setting of the metasedimentary rocks from the basal allochthonous units of NW Iberia (Variscan suture, Galicia). Lithos 146, 196–208.

Harpum, J., Brown, P.E., 1958. Quarter Degree Sheet 71 S.W. Geol. Surv.. Dodoma.

Kasanzu, C.H., Maboko, M.A.H., Manya, S., 2016a. Reconstruction of Pliocene-Pleistocene sediment sources and weathering intensity in the paleo-life rich Olduvai and Laetoli basins of northern Tanzania using major and trace element geochemistry and Sr isotopic data. Journal of African Earth Sciences 123, 89–98.

Kasanzu, C.H., Linol, B., de Wit, M., Brown, R., Persano, C., Stuart, M.F., 2016b. From source to sink in Central Gondwana: coeval exhumation of the Precambrian basement rocks of Tanzania and sediment accumulation in the adjacent Congo Basin. AGU, Tectonics. http://dx.doi.org/10.1002/2016TC004147.

Kasanzu, C., Maboko, M.A.H., Manya, S., 2008. Geochemistry of fine grained clastic sedimentary rocks of the Neoproterozoic Ikorongo Group, NE Tanzania: implications for provenance and source rock weathering. Precambrian Research 164, 201–213.

Kazimoto, O.E., Shenk, V., Appel, P., 2015. Granulite-facies metamorphic events in the northwestern Ubendian Belt of Tanzania: implications for the Neoarchean to paleoproterozoic crustal evolution. Precambrian Research 256, 31–47.

Lawley, C.J.M., Selby, D., Condon, D.J., Horstwood, M., Millar, I., Crowley, Q., Imber, J., 2013. Lithogeochemistry, geochronology and geodynamic setting of the Lupa-Terrane, Tanzania: implications for the extent of the Archean Tanzanian Craton. Precambrian Research 231, 174–193.

Lenoir, J.L., Liegois, J.P., Theunissen, K., Klerkx, J., 1994. The paleoproterozoic Ubendian shear belt in Tanzania: geochronology and structure. Journal of African Earth Sciences 19, 169–184.

Manya, S., 2011. Nd-isotopic mapping of the Archaean–Proterozoic boundary in southwestern Tanzania: implication for the size of the Archaean Tanzania Craton. Gondwana Research 20, 325–334.

Manya, S., 2012. SHRIMP zircon U–Pb dating of the mafic and felsic intrusive rocks of the Saza area in the Lupa goldfields, southwestern Tanzania: implication for gold mineralization. Natural Science 4, 724–730.

Manya, S., 2013. Geochemistry and U-Pb zircon dating of the high-K calc-alkaline andesitic lavas from the Buanji Group, south-western Tanzania. Journal of African Earth Sciences 86, 107–118.

Manya, S., 2014. Geochemistry of the palaeoproterozoic gabbros and granodiorites of the Saza area in the Lupa Goldfield, southwestern Tanzania. Journal of African Earth Sciences 100, 401–408.

McLennan, S.M., 1989. Rare earth elements in sedimentary rocks: influence of provenance and sedimentary processes. In: Lipin, B.R., MacKay, G.A. (Eds.), Geochemistry and Mineralogy of Rare Earth Elements. Mineralogical Society of America, 169–639, 200.

Nagarajan, R., Madhavaraju, J., Nagendra, R., Selvamony, J., Altrin, A., Moutte, J., 2007. Geochemistry of Neoproterozoic shales of the Rabanpalli Formation, Bhima Basin, northern Karnataka, southern India: implications for provenance and paleoredox conditions. Revista Mexicana de Ciencias Geológicas 2, 150–160.

Nesbitt, H.W.M., Young, G.M., 1982. Early Proterozoic climates and plate motions inferred from major element chemistry of lutites. Nature 299, 715–717.

Nesbitt, H.W., Young, G.M., 1984. Prediction of some weathering trends of plutonic and volcanic rocks based on thermodynamic and kinetic considerations. Geochimica et Cosmochimica Acta 48, 1523–1534.

Roddaz, M., Viers, J., Brusset, S., Baby, P., Boucayrand, C., Hérail, G., 2006. Controls on weathering and provenance in the Amazonian foreland basin: insights from major and trace element geochemistry of Neogene Amazonian sediments. Chemical Geology 226, 31–65.

Servaraj, K., Arthur, C.C., 2006. Moderate chemical weathering of subtropical Taiwan: constraints from solid-phase geochemistry of sediments and sedimentary rocks. The Journal of Geology 114, 101–116.

Shao, J., Yang, S., Li, C., 2012. Chemical indices (CIA and WIP) as proxies for integrated chemical weathering in China: inferences from analysis of fluvial sediments. Sedimentary Geology 265–266, 110–120.

Sun, S.S., McDonough, W.F., 1989. Chemical and isotopic systematic of oceanic basalts: implication for mantle composition and processes. In: Saunders, A.D., Norry, M.J. (Eds.), Magmatic in Ocean Basins, Geol. Soc. of Lond. Spec. Pub, vol. 42, pp. 313–345.

Taylor, S.R., McLennan, S.M., 1985. The Continental Crust: its Composition and Evolution. Blackwell, Oxford, UK. Blackwell Sci. Pub, 312 pp.

Tulibonywa, T., Manya, S., Maboko, M.A.H., 2015. Paleoproterozoic volcanism and granitic magmatism in the Nguala area of the Ubendian Belt, SW Tanzania: constraints from SHRIMP zircon U-Pb ages and Sm-Nd isotope systematics. Precambrian Research 256, 120–130.

Zhao, G., Sun, M., Wilde, S.A., Li, S., 2004. A Paleo-mesoproterozoic supercontinent: assembly, growth and breakup. Earth-Science Reviews 67, 91–123.